Global Solar Energy, Inc.
5575 South Houghton Road
Tucson, Arizona 85747
(520) 546-6313 (Voice)
(520) 546-6318 (FAX)

"Tolerance of Three-Stage CIGS Deposition to Variations Imposed by Roll-to-Roll Processing"

Phase II Annual Report
May 2003 – May 2004
Thin Film Partnership Subcontract # ZDJ-2-30630-14

Prepared by: **M.E. Beck, Global Solar Energy, Inc.**
I.L. Repins, , ITN Energy Systems, Inc.

Executive Summary

Co-evaporation of $CuIn_xGa_{1-x}Se_2$ (CIGS) via two-stage and three-stage processes has been used in a variety of laboratories throughout the world to produce small-area devices with efficiencies greater than 15%. Thus, these deposition methods have come to be viewed as laboratory standards for the formation of CIGS absorbers used in respective photovoltaic devices. Although quite successful and relative easy to implement on a small R&D scale, scale-up to a commercially viable level proves to be rather challenging, as a number of conditions are encountered during continuous manufacturing that differ from the laboratory process. Such differences include both those imposed by continuous processing of moving substrates, and those implemented to decrease costs and increase throughput. It is therefore beneficial to understand the tolerance of the established laboratory processes to variations in deposition procedures.

Research under this program consists of four basic parts to examine the tolerance of the established laboratory process to variations in deposition procedures:

1. Setting up the National Renewable Energy Laboratory (NREL)-developed three-stage CIGS laboratory process in a bell jar. (Phase I)
2. Characterizing the GSE roll-to-roll production chambers and device finishing steps in terms of the variables important to the laboratory processes. (Phase II)
3. Using the bell jar system to step incrementally from the NREL process to the conditions experienced by a sample during manufacturing, and characterizing the resulting films and devices. (Phase II and III)
4. Applying the process sensitivity information gained from the bell jar system to the production systems to realize improved device performance, yield, and process robustness. (Phase II and III)

Work during Phase II progressed in three major areas: production system characterization, quantification of process sensitivities in the bell jar, and application of results to the production roll-coaters. To form a complete picture of conditions in the production systems, metals flux profiles as a function of Se pressure were documented, Se impingement rates were derived from sensor data, and thermocouple data was used to estimated temperature profiles. In the bell jar, the impact of the following process variations on device performance were quantified: CIGS cool-down rate, cool-down Se flux, venting temperature, shortened time between venting and CdS, maximum Cu ratio, and final Cu ratio. Related to production systems, the following topics were investigated: process robustness and device performance as a function of maximum and final Cu ratio, real-time sensing of maximum Cu ratio, effect of processing delays between CIGS and CdS, transparent conducting oxide stability with exposure to damp heat, and improved junction formation via thioacetamide treatment.

Phase III tasks will build on this year's results: In the bell jar, several process sensitivity investigations will be concluded, and some new ones begun. These investigations will include use of less expensive source materials, decreased deposition times, variations in instantaneous Se to metals ratio as implied by the roll-coater flux profiles, optimization of Na precursor at roll-coater conditions, and CdS optimization. Where applicable, these new results will be applied in the production roll-coaters to demonstrate performance and yield improvement. Appropriate actions based on this year's maximum Cu ratio and thioacetamide treatment data will also be defined and implemented.

TABLE OF CONTENTS

LIST OF FIGURES

LIST OF TABLES

1 Introduction

1.a Background

Co-evaporation of $CuIn_xGa_{1-x}Se_2$ (CIGS) via two-stage and three-stage processes has been used in a variety of laboratories throughout the world to produce small-area devices with efficiencies greater than 15%.[1,2,3,4,5] Thus, these deposition methods have come to be viewed as laboratory standards for the formation of CIGS absorbers used in respective photovoltaic (PV) devices. Although quite successful and relative easy to implement on a small R&D scale, scale-up to a commercially viable level proves to be rather challenging, as a number of conditions are encountered during continuous manufacturing that differ from the laboratory process. Such differences include both those imposed by continuous processing of moving substrates, and those implemented to decrease costs and increase throughput. It is therefore beneficial to understand the tolerance of the established laboratory processes to variations in deposition procedures.

Only limited information is available in the literature addressing the tolerance of the laboratory processes to several variations. Some studies have been published related to CIGS thickness,[6] maximum deposition temperature and time spent by the film in the Cu-rich stage,[7,8] Na content,[9,10] rate profiles,[11] and final overall Cu/(In+Ga) atomic ratio.[12] Not only are there additional, at times more important, absorber characteristics that define the quality of the resulting absorber for use in a PV device, but these experiments were conducted without correlation to practical commercial fabrication methods. Further variations to the deposition procedure may be encountered in the manufacturing environment and include:

- Further shortened overall deposition times,
- Instantaneous variations in the Se/metals flux ratio outside the typically-recommended envelope due to spatial distribution of metallic flux,
- Impurities expected from less expensive, less pure source materials or alternative substrates,
- Deviation of initial film temperature from the prescribed two- and three-stage values,
- Variation in the fraction of group III elements deposited in the first versus third stages,
- Variations in sample cool-down procedures and post-CIGS handling, and
- Exposure to species outgassed and reflected from hot chamber walls.

Global Solar Energy, Inc. (GSE) and lower-tier subcontractor ITN Energy Systems, Inc. (ITN) are addressing these process tolerance issues in this program. The definition and resolution of process tolerance issues satisfy many of the goals of the Thin Film Photovoltaics Partnerships Program (TFPPP). First, the investigation is likely to identify acceptable ranges for critical deposition parameters. This will have the benefit of providing upper and lower control limits for in-situ process monitoring components, thus increasing average efficiency as well as yield of product. Second, the exploration may uncover insensitivities to some processing procedures, allowing manufacture of modules at increased throughput and decreased cost. The exploration allows a quantitative evaluation of the trade-offs between performance, throughput, and costs. Third, the proposed program also satisfies the TFPPP goal of establishing a wider research and development base for higher-efficiency processing. Fourth, the acquisition of data defining sensitivity to processing has important implications for the required accuracy of process sensors and control. Finally, the program helps the photovoltaic community advance toward a better understanding of CIGS growth, a longer-term goal of the TFPPP.

1.b Approach

The approach to address the issues mentioned above consists of four basic parts:

1. Setting up the NREL-developed three-stage laboratory process in a bell jar at ITN.
2. Characterizing the roll-to-roll (RTR) production chambers at GSE in terms of the important variables.

3. Using the bell jar system to step from the NREL process to the conditions experienced by a sample during roll-to-roll manufacturing, and characterizing the resulting films.
4. Utilizing the process sensitivity information gained in the bell jar system in the production chambers.

These four tasks are being performed roughly in the order listed. During Phase I, a three-stage bell jar process was established at ITN, characterization of the GSE RTR production processes began, and the bell jar system was used to explore some sensitivities of the three-stage process. During Phase II, characterization of the GSE RTR production processes in terms of major variables was completed, further process sensitivities were explored in the bell jar, and application of process tolerance information to the roll-coaters began. Progress on each Phase II task is described in following sections.

2 Roll-Coater Characterization

A major task under this program was characterizing the roll-to-roll production chambers at GSE in terms of the variables known to be important to the three-stage process. For CIGS deposition, those variables include substrate temperature as a function of time, as well as Cu, In, Ga, and Se fluxes as a function of time. Information relating each of these quantities in the roll-coaters to its counterpart in the bell jar has been obtained and is described below. In short, 1) metals flux profiles were found to agree well with the expected $\cos^3\theta$ distribution and are unaffected by Se pressures, 2) Se impingement rates were derived from sensor data, and 3) thermocouple data was used to estimated temperature profiles.

2.a Metals Flux Profiles with Se

In Phase I, production evaporation source flux profiles were characterized,[13] and found to agree well with the expected[14] $\cos^3\theta$ distribution. However, it was unknown whether interaction between background Se pressure and the metals plume would change the metals flux profile. Thus, experiments were performed to determine the degree and manner in which interaction between the selenium and copper vapor plumes affects the peak intensity and shape of the copper flux distribution at the web under conditions used for CIGS production at GSE.

To best utilize available chamber time, measurements of the copper plume distribution as a function of selenium backpressure were carried out in the intelligent processing (IP) chamber at ITN, using a version of the GSE production sources. The basic approach was to establish a fixed copper effusion rate and selenium back pressure, move a fresh section of web quickly into the deposition zone, stop the web to allow copper (and selenium) to accumulate, move the web quickly out of the deposition zone, and measure the thickness of copper deposited onto the web as a function of position using XRF. To produce results that could be related to processing parameters used at GSE, efforts were made to ensure that both containment of selenium and measurement of the selenium in the IP chamber were as similar as possible to the containment and measurement at GSE.

Imprints of the copper flux distribution were made on the web three times during the run. Each time, this imprinting was done as follows:

1. The web was moved forward at 20 inches per minute for at least 28 inches to bring fresh web into the deposition zone.
2. The web was stopped and held in place for a period of 20 minutes.
3. The web was moved forward at 20 inches per minute for at least 28 inches to entirely remove the newly coated section of web from the deposition zone.

During imprinting, the copper source was operated at a setpoint temperature resulting in an effusion rate suitable for deposition of a 2 μm-thick CIGS film at a web speed of about 0.75 inches per minute. Heaters and neighboring sources were held at temperatures comparable to those used during depositions, so that – like during deposition – these elements did not condense Se out of the cloud.

This procedure produced sections with copper thicknesses consisting of an imprint of the copper flux distribution superimposed on a uniform background, which is the thickness of copper deposited on a web moving continuously through the deposition zone at 20 inches per minute. This analysis assumes that the sticking coefficient for copper vapor incident on

the web is uniform, and that the copper flux distribution remains constant throughout the 23-minute procedure. The first imprint was made once the Se signal appeared to have stabilized at an intermediate value (termed "level 2 Se flux"). The selenium signal was then increased ("level 3" Se). The second imprint was made after this adjustment yielded a relatively stable Se signal. The selenium signal was then adjusted once more to allow for the final desired lowest Se signal ("level 1") to stabilize prior to obtaining the last measurement – i.e., making the last imprint. Following the run, the thicknesses of copper and selenium were measured by XRF for each imprinted region of web along the strip that passed directly over the copper nozzle. These measurements were carried out at intervals of 0.63 inches across the entirety of each of the three imprinted regions.

Thicknesses of copper in the films deposited on the web as measured by XRF are plotted as a function of down-web position for each of the three imprint regions in Figure 1. Positions zero and 27.75 correspond the boundaries of the selenium containment zone. The location of the copper source is also shown. Note, however, that the copper source may not have been precisely level, i.e., its nozzle may not have been completely vertical. This could account for a small offset between the nozzle location and the peak of the thickness distributions. The increase in thickness at the 30-inch position for the level 2 data is due to this portion of web being "parked" in the deposition zone prior to making the imprint. Note that most of the data for positions outside of the deposition zone are at or slightly below zero. This should not strictly be the case, as all parts of the web must have accumulated some copper while traveling through the deposition zone at 20 inches per minute. By integrating the curves in the figure, one can calculate that this minimum amount of accumulation should be between 60 to 80 Å. The discrepancy must be attributed to zero-offset error in the XRF analysis.

The XRF measurements also gave values for the effective thickness of selenium in the films. The selenium and copper thicknesses were combined to determine the ratio of the atomic concentration of selenium to that of copper, as plotted in Figure 2. It is interesting to note that most of the deposited Se exists in either a 1:2 or 1:1 ratio with the Cu. These ratios are the same as those of the compounds Cu_2Se and CuSe, respectively. The very high Se/Cu values at the edges of the distributions may be due to the increased importance of XRF measurement errors to Se/Cu ratio as the Cu thickness approaches 0. No independent phase analysis was performed to identify phases present, as this was not the goal of the investigation.

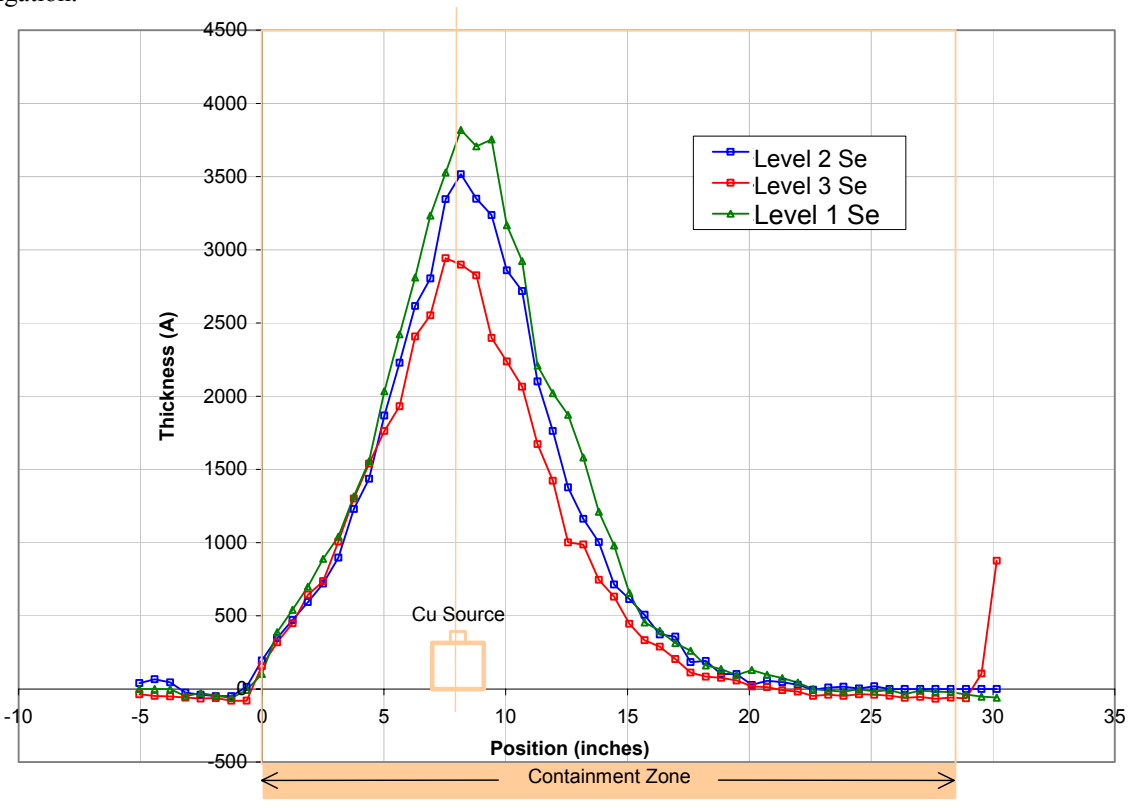

Figure 1: Copper thickness measured by XRF as a function of position for the three ranges during which an imprint was made.

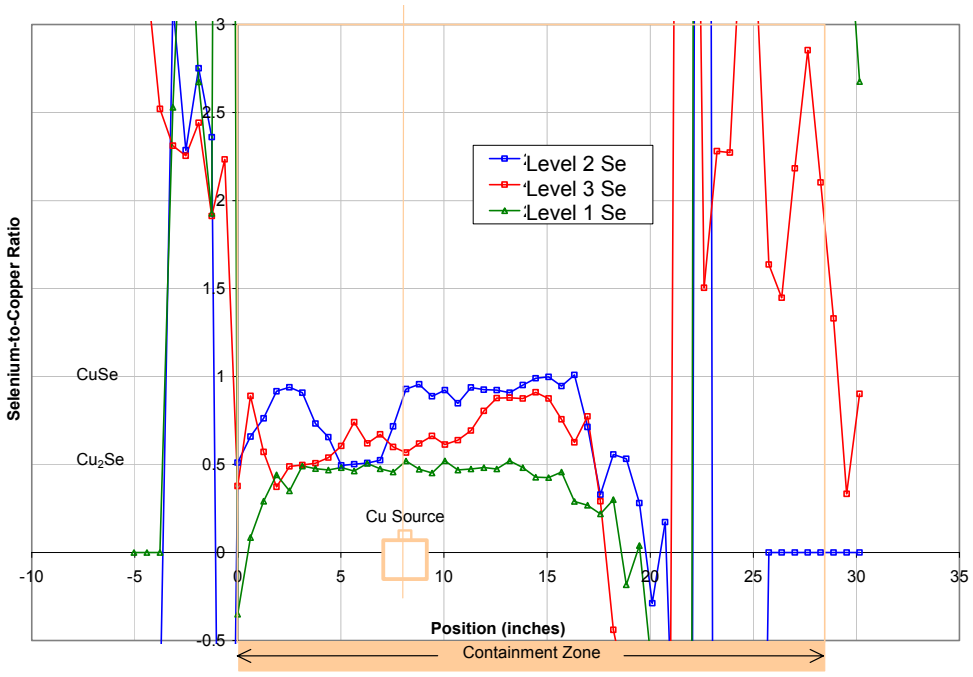

Figure 2: Ratio of selenium-to-copper atomic concentrations as a function of position.

Clearly, the primary observed effect of higher selenium signal on the copper flux was an overall decrease in its intensity. The effect of selenium on the shape of the flux distribution is best seen in Figure 3, in which each flux profile was normalized with respect to its peak value. This figure reveals that there were no significant changes in the shape of the distributions. For the highest-signal range (level 3), there may have been a slight shift towards the up-web side of the deposition zone, although the magnitude of the shift is comparable with the uncertainty in determining the web position (~0.5 inches). As the selenium source is located on the down-web side of the deposition zone, the direction of the observed shift is consistent with displacement of the copper plume due to the directed component of the selenium vapor.

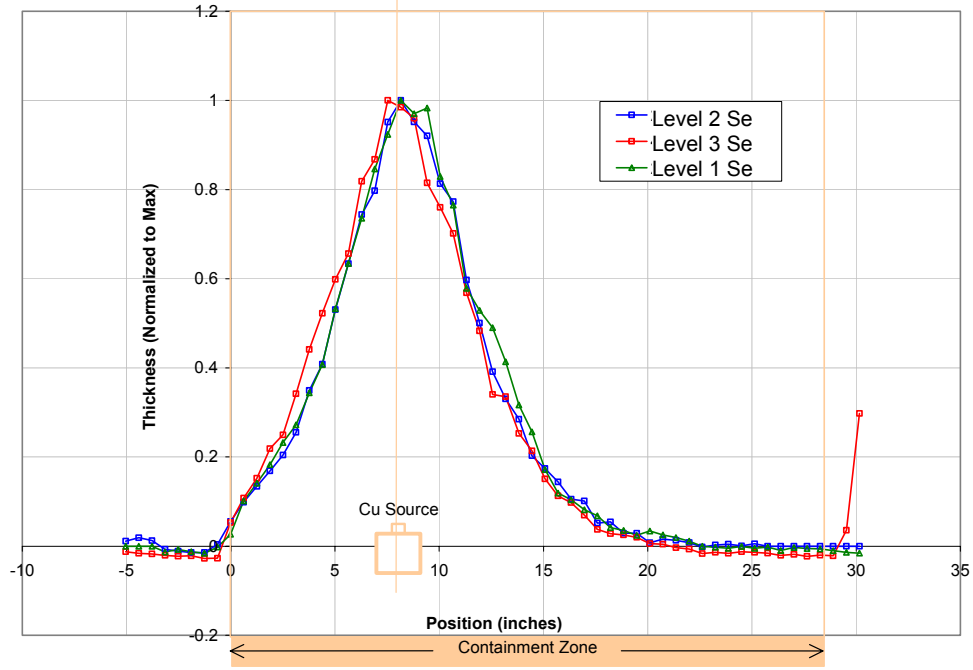

Figure 3: Copper thickness normalized to the peak value for each range.

Measurements at the Institute of Energy Conversion (IEC) using a hoop apparatus have determined that the flux for effusion of copper from a nozzled boat with no selenium present varies as the cube of the cosine of the angle to the nozzle centerline. For the present experiment, in which selenium comparable to the amount used at GSE was present, the copper thickness data again exhibit the $\cos^3$ angular dependence. Figure 4 shows the copper thickness data for each signal range together with fits to the data based on a $\cos^3$ angular distribution taking into account the geometric factors that convert the distribution from a function of θ to a function of position along the web. The fitting was performed using data between the 1-inch and 25-inch positions and with the overall magnitude and the center position of the distribution being the only fitting parameters. Fitting was also performed with the exponent of the cosine added to the list of fitting parameters – i.e. the data were fit using a $\cos^n$ angular distribution. The resulting best-fit values are shown in Table 1. The best-fit values for the exponent are very close to $n = 3$, and the curves produced from this fit are hardly distinguishable from the $\cos^3$-fit curves shown in Figure 4.

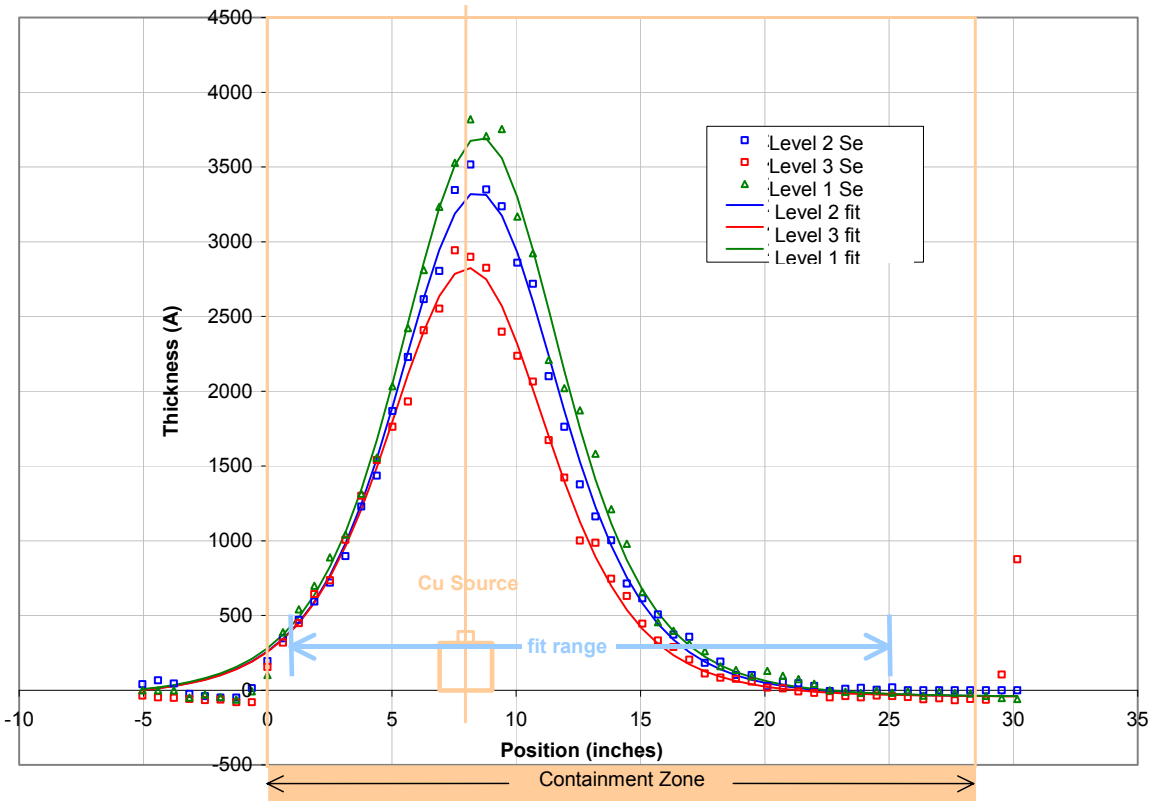

Figure 4: Cosine-cubed flux distributions with magnitudes and peak centers fit to the copper XRF thickness data for each signal range.

Fit Parameter	*Units*	*level2*	*level3*	*level1*
Magnitude	Å	3414	2854	3742
Center	Inches	8.45	8.06	8.54
N (exponent)		3.24	2.87	2.97

Table 1: Fit parameter values resulting from fitting copper XRF thickness data to the "cosine^n" flux distribution with the magnitude, peak center, and exponent (i.e. 'n') of the distribution as the only fitting parameters.

2.b Se rates

During Phase II, fundamental principles were used to translate data from proprietary sensors in the roll-coaters to an impingement rate in Å/sec. Results are roughly consistent with earlier rate estimates based on Se consumption as a function of metals rates. The comparison lends credibility to both methods of mapping the Se in the roll-coaters.

2.c Temperature

Roll-coater temperature profiles were estimated from thermocouple data. These data include both heater temperatures and temperatures recorded from thermocouples tack-welded to the stainless steel web as they traveled through the deposition system. Although these data only estimate the actual web temperature, since film emissivity and radiation from sources may cause some differences during deposition, the apparent insensitivity of bell jar device efficiencies (see section 3.b, "Deposition Temperature and Maximum Cu Ratio") to slight temperature changes suggest that these estimates are sufficient.

3 Bell Jar Process Sensitivities

A second major task in this program is using the bell jar to quantify three-stage process sensitivities that pertain to roll-to-roll manufacturing. During Phase II, the subjects of these examinations have included post-deposition treatments (such Se flux during cool-down), deposition temperature, maximum Cu ratio, instantaneous Se-to-metals ratio, reproducibility, and comparisons with NREL devices.

3.a Post-CIGS Deposition Conditions

A number of procedures subsequent to application of Cu, In, and Ga fluxes may affect device performance. Laboratory procedures often specify sample cool-down rates, Se flux during cool-down, maximum venting temperature, and maximum time between CIGS deposition and CdS. Such procedures are often based on trials involving very few devices, untested but established routines, or anecdotal evidence. In this section, impact of such procedures is quantified.

The effect of CIGS chamber venting temperature was examined as to its potential impact on device efficiency. Although typical laboratory procedures call for cooling CIGS substrates to near room temperature before venting the CIGS chamber, higher venting temperatures are desirable for maximizing throughput. To investigate this issue, nominally identical CIGS depositions were performed on 3" × 3" glass substrates in the bell jar. After deposition, the substrate was allowed to cool in vacuum for varying amounts of time. Device efficiency as a function of venting temperature is shown in Figure 5. Green circles show individual device efficiencies from each of 89 devices on 10 substrates. Dark blue data points are the average efficiency for each condition, with error bars showing ± one standard deviation. For the highest venting temperature (300°C), a slightly different procedure was followed to prevent significant formation of H_2Se. At 300°C, the hi-vac valve was closed to stop pumping and allow gradual leak-up of chamber pressure, but chamber was not fully vented until cool. In each case, there is no measureable impact of the venting temperature on device performance. For all device parameters reported in this document, measurement conditions are AM1.5, total-area, without anti-reflective coating.

The effect of post-deposition CIGS cool-down conditions was also examined for impact on device efficiency. Two effects are of concern when considering sample cool-down after CIGS deposition. The first is Se rejection. Laboratory samples are typically cooled slowly while applying Se flux[15] to prevent Se loss from the hot film. The second effect of concern is a possibly beneficial Se anneal[16] as the film is exposed to high temperature and Se for an extended period post-deposition. To quantify the impact of these effects, CIGS was deposited on 3" × 3" substrates utilizing the same conditions up to the end of the third stage. After the end of the third stage, samples were allowed to cool at different rates. Under the first cool-down condition, the samples spent 200 seconds above 400°C, the maximum cooling rate of glass in the bell jar. Under the second cool-down condition, the samples spent 250 seconds above 400°C. Se flux was either turned off immediately at the end of stage 3, or delivered at the stage 3 rate until the substrate temperature dropped below 400°C. As a final variation, a Se anneal (180 seconds at 550 °C) was performed prior to cool-down. Results from each variation are summarized in Figure 6. Red circles show individual device efficiencies from each of 127 devices on 11 substrates. Dark blue data points are the average efficiency for each condition, with error bars showing ± one standard deviation. Conditions

in Figure 6 correspond to those typically utilized in the laboratory and in production. Over the range explored, there is no measureable impact of the cool-down conditions on device performance.

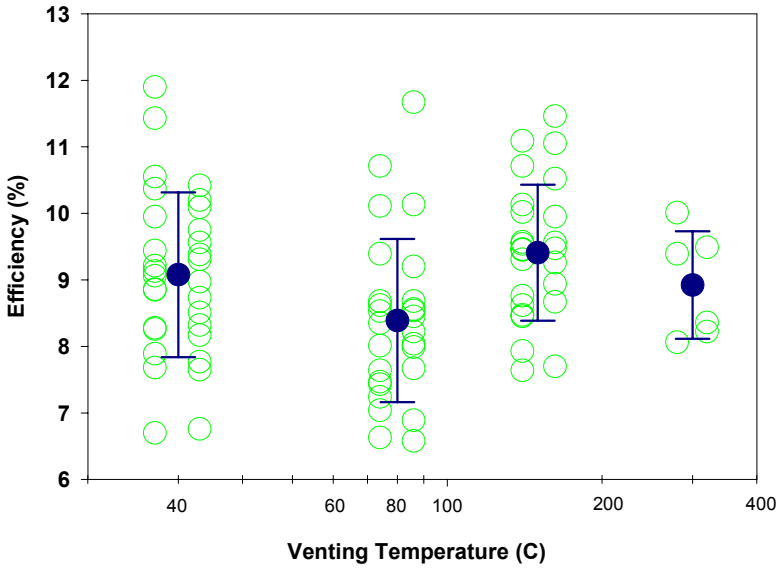

Figure 5: Device efficiency as a function of venting temperature.

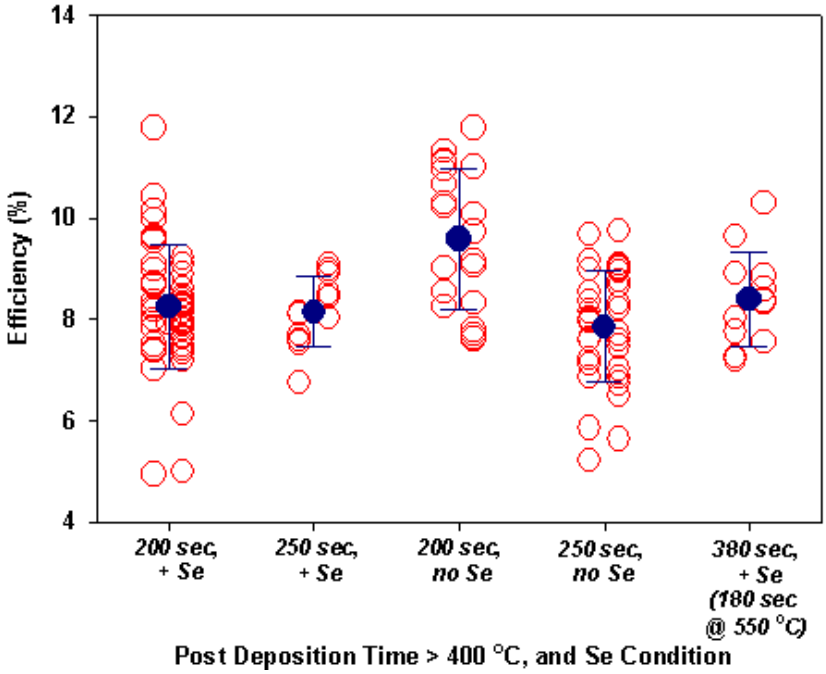

Figure 6: Device efficiency as a function of post-CIGS deposition cool-down conditions.

Impact of delay time between CIGS and CdS depositions on device performance was also examined. While longer delay times were examined using the roll-coaters (see section 4.b, "Post-CIGS Deposition Conditions"), the bell jar was utilized to examine air exposure times shorter than those currently practical on the production floor. Each sample in the study was deposited using standard three-stage conditions. Upon venting, the sample was quickly removed from the chamber and cut in half in the direction perpendicular to composition gradients. The "rushed half" was immersed in the

waiting CdS bath within three minutes of first air exposure, while – for maximum contrast – the "delayed" half was stored in air for two weeks before receiving CdS. JV characteristics for two such trials are shown in Figure 7. For sample #1, the rushed CdS half shows the JV curve inflection that has been associated with oxidation, band offsets, interface states acting as a barrier at the CdS/CIGS interface (black curve).[17,18] Furthermore, the rushed CdS sample is not stable. A second measurement, taken three weeks later (green curve), is markedly different. The delayed half of the sample (red and yellow curves) shows no such effects. For sample #2, the rushed half (blue curve) exhibited standard behavior, suggesting that the effect of reducing air exposure time is very sensitive either to ambient conditions (such as humidity) or to CIGS properties – e.g., degree of In and Ga at the surface, associated oxide formation, and subsequent bath chemistry interactions.[19] In any case, no efficiency gain was realized by shortening the time between venting and CdS. Furthermore, in one case, metastability and decreased efficiency were associated with the decreased time before CdS.

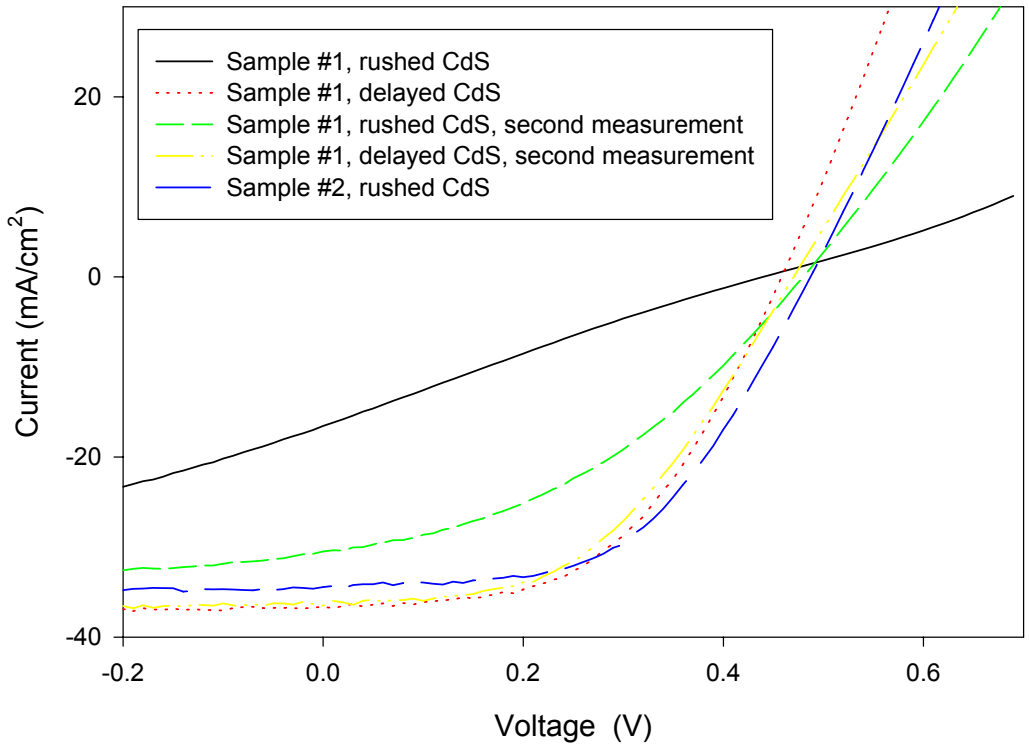

Figure 7: Current-voltage characteristics of baseline CIGS with rushed or delayed CdS.

3.b Deposition Temperature and Maximum Cu Ratio

CIGS deposition temperatures were varied in the bell jar to assess the impact of straying from process setpoints on device performance. During this examination, it was discovered that unintentional variations in maximum Cu ratio (i.e. the atomic ratio Cu/group III at the end of the second stage) had a stronger effect on device efficiency than the intentional temperature variations. Specifically, it was found that

- For devices with low final Cu ratio ($R_3 \leq 0.9$), device efficiency improves continuously with maximum Cu ratio approaching 1.15.
- By the time maximum Cu ratio reaches 1.3, a significant decrease in efficiency is observed.
- Efficiency falls off as final Cu ratio approaches 1, but some samples tolerate a higher final Cu ratio than others. However, the controlling condition for limit on maximum final Cu ratio is not apparent from the present data.

The importance of a Cu-rich growth period has been the subject of some disagreement in the literature, with various studies confirming its importance,[12,20,21,22] and others finding it important only under specialized circumstances.[6,7,8] Since the Cu-rich period enhances growth kinetics via existence of liquid copper selenide, it is therefore surmised that Cu-rich growth is most important in situations where grain growth encounters other unfavorable conditions, such as fast deposition rates, low temperatures, or unoptimized supply of Na. Thus, the bell jar findings described in the paragraphs below are currently being revisited using Ga content and deposition rates as similar as possible to those in the roll-coaters.

Device parameters were analyzed as a function of maximum and final Cu ratio for 75 devices on 25 substrates. As the 25 substrates were taken from studies involving intentional variations in temperature, venting, and cool-down procedures, such variations are expected to add some scatter to the Cu-ratio analysis. However, it is apparent that the intentional variables are not the strongest influence on device efficiency. For each 3" × 3" substrate, several pieces of information were tabulated. Grids were oriented relative to position in the chamber. Device results at the center, the Ga boat front corner (most Cu rich), and the In boat back corner (most Cu-poor) were recorded. Each of these device results were associated with a final Cu ratio, based on the XRF measurement at the film center, and on earlier examinations of Cu ratio nonuniformity. It was estimated that the Cu ratio for the Ga front corner device is 5% larger than that of the center device, and the Cu ratio for the In back corner device is 5% smaller than that of the center device. Next, logged flux profiles were used to convert each final Cu ratio ("R_3") to a maximum Cu ratio ("R_2"). Assuming a constant group III deposition rate in stages 1 and 3, the maximum Cu ratio for any device is

$$R_2 \cong R_3 \times (\text{stage 1 + stage 3 deposition time})/(\text{stage 1 deposition time}) \qquad (i)$$

Two major trends are apparent. First, for devices with low final Cu ratio ($R_3 \leq 0.9$), device efficiency improves continuously with maximum Cu ratio approaching 1.15. These data are shown in Figure 8. Points from the same substrate are connected by lines. Some points in Figure 8 are not connected in a set of three, as the other devices on the substrates either did not satisfy the condition $R_3 \leq 0.9$, or were shunted. (Devices are deduced to be shunted by localized defects if fill factor is less than 40%, and efficiency at least 2% less than the neighboring device.) 10% devices were only produced with maximum Cu ratio exceeding 1, and 11%+ devices were only produced with maximum Cu ratio exceeding 1.05. Efficiency loss for lower Cu ratios is spread comparably over V_{oc}, and fill factor. Device parameters for the efficiency data of Figure 8 are shown in Figure 9.

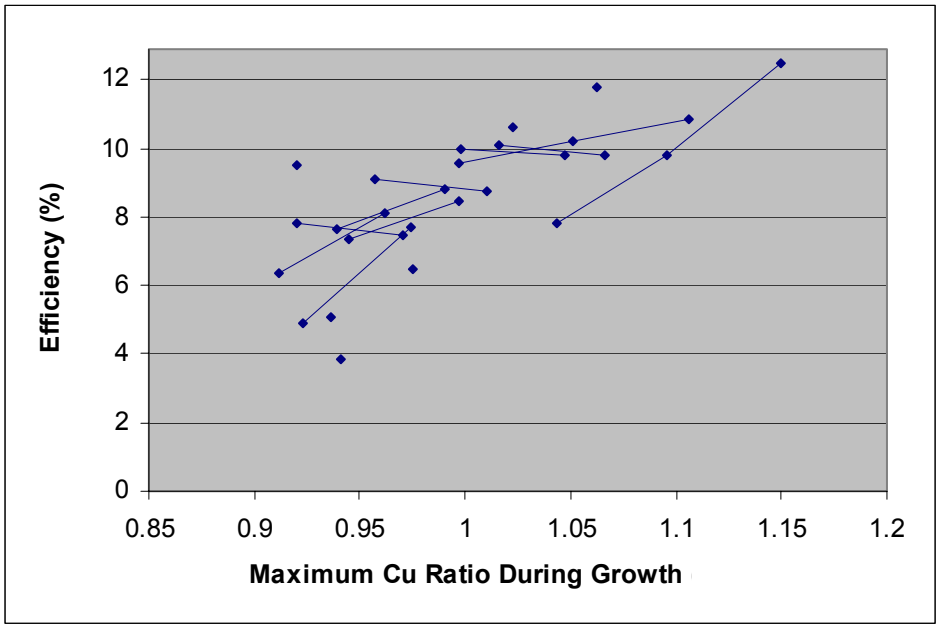

Figure 8: Efficiency as a function of maximum Cu ratio for devices with final Cu ratio ≤ 0.9.

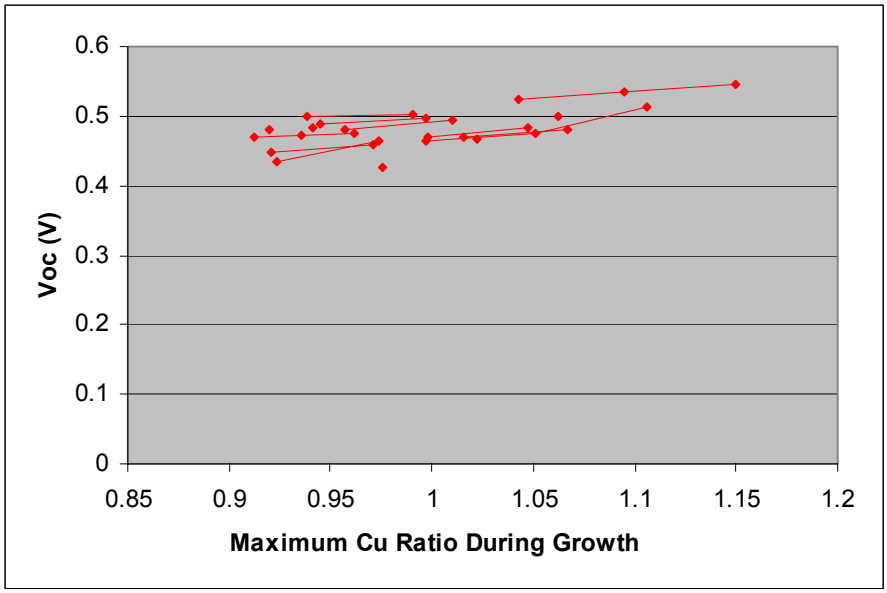

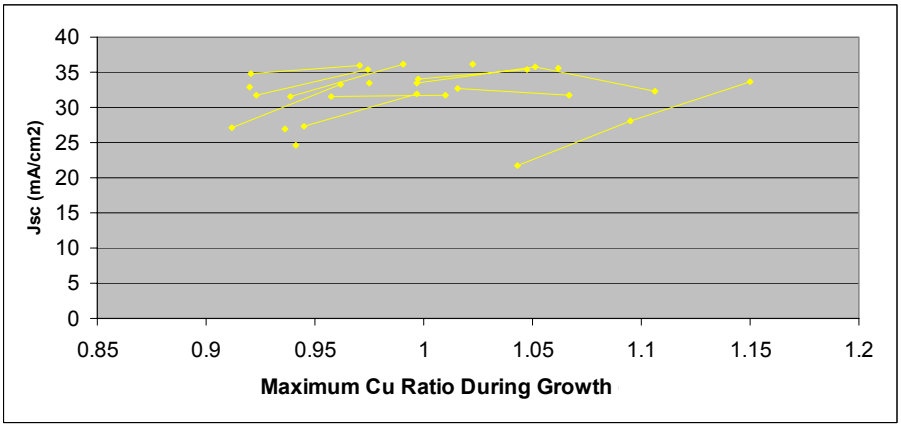

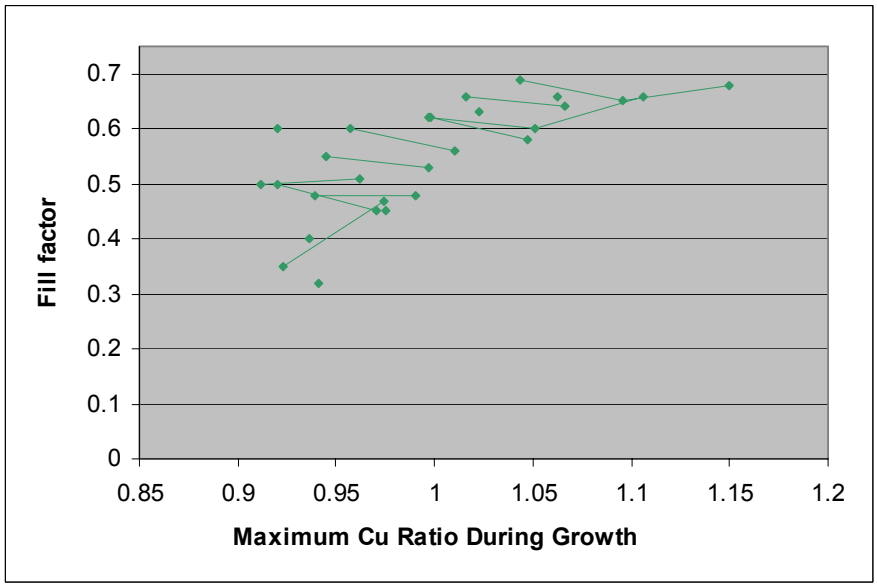

Figure 9: Device parameters for efficiency data shown in previous figure.

The second trend apparent in the data is that efficiency falls off as final Cu ratio approaches 1, but some samples tolerate a higher final Cu ratio than others. Figure 10 shows efficiency as a function of final Cu ratio for all samples in the study. At present it is unclear whether tolerance of a high final Cu ratio is a function of the maximum Cu ratio, or other variables in the study. Given that there seems to be no efficiency penalty for final Cu ratios in the range 0.8 to 0.9 (based on this and other[12] studies), it is currently recommended that CIGS films be produced with a final Cu ratio less than or equal to 0.9.

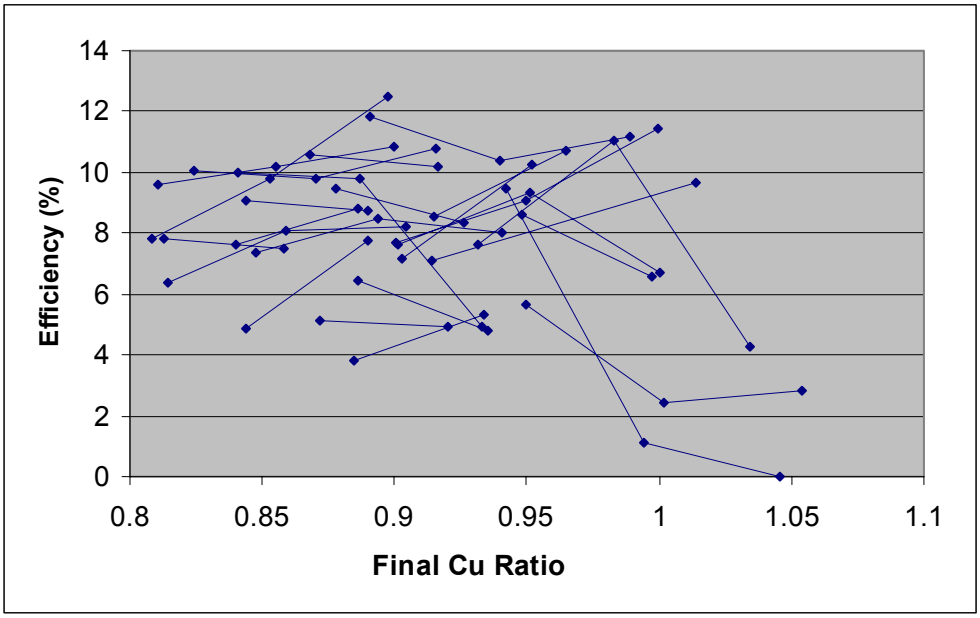

Figure 10: Efficiency as a function of final Cu ratio for all devices in study.

After the above trends in efficiency were recognized, four CIGS depositions were performed to determine an acceptable processing window for maximum Cu ratio. Devices with maximum Cu ratios (i.e. Cu ratio at the end of stage 2) between 1.2 and 1.4 exhibited low open-circuit voltages, and efficiencies near 5%.

X-axis uncertainty in Figure 8 and related graphs is considerable. The final composition of the film center is repeatable to within ±1%, due to noise in the XRF. Furthermore, the Cu ratio gradient across the sample may change slightly from run to run, due to boat positioning, film Ga content, and grid registration. Thus, the final composition ratio of the corner devices carries and additional approximate ±2% uncertainty. Deduction of maximum Cu ratio from final Cu ratio introduces further uncertainty. Use of equation (i) assumes constant group III deposition rates throughout stage 1 and 3. In some instances, this assumption is clearly not valid. For example, in some depositions, the Ga rate in stage 3 reaches its setpoint prior to the In rate. Thus, if the In deposition time is used as the stage 3 time, the maximum Cu ratio is underestimated. Furthermore, it is possible that drift in the EIES calibration – perhaps a function of temperature or Se pressure – occurs over the course of the deposition.

As mentioned in the preceding paragraphs, device performance variations seen during a study of temperature variations were actually dominated by the maximum Cu ratio during growth. When temperature differences are noted on the data from Figure 8, the data appear as shown in Figure 11. Here, devices fabricated at the same temperatures are shown in the same colors. The red line shows a second-order least-squares fit to all the data, which can be used to account for the effect of maximum Cu ratio. Devices above the red line are more efficient than average, and devices below the red line are less efficient than average. Figure 12 shows, for each first stage temperature, the average distance the data points fall above the red fit line. No trend is apparent.

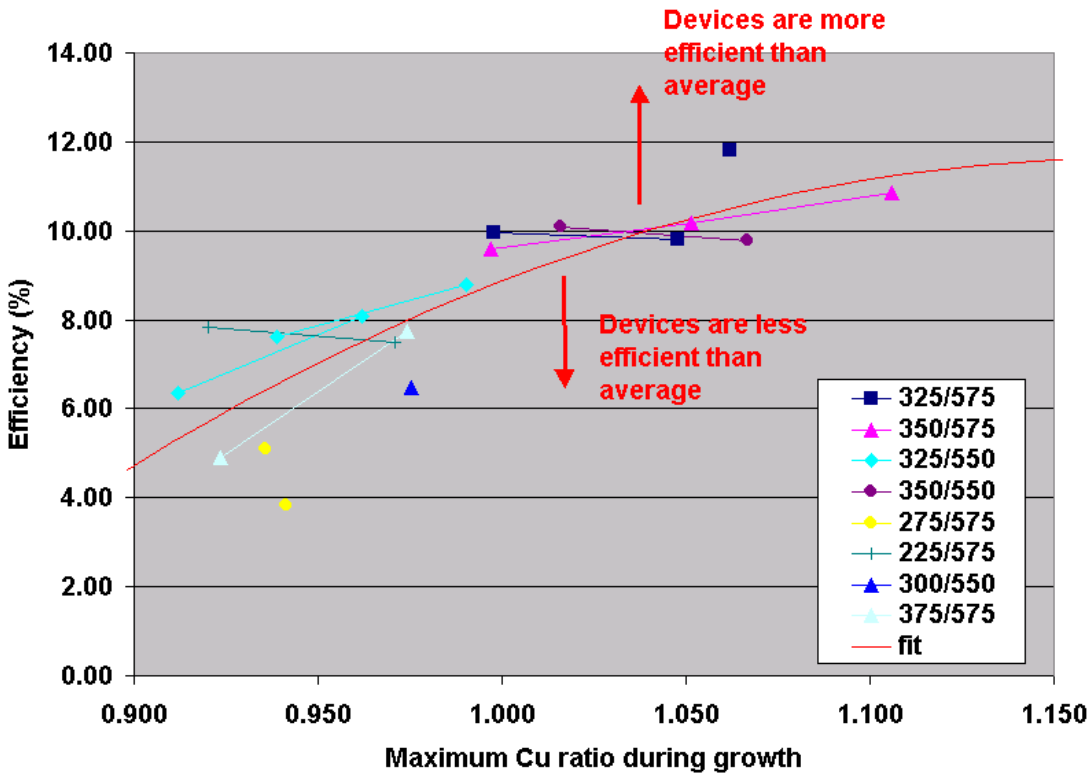

Figure 11: Efficiency as a function of maximum Cu ratio and temperature for devices with final Cu ratio < 0.9.

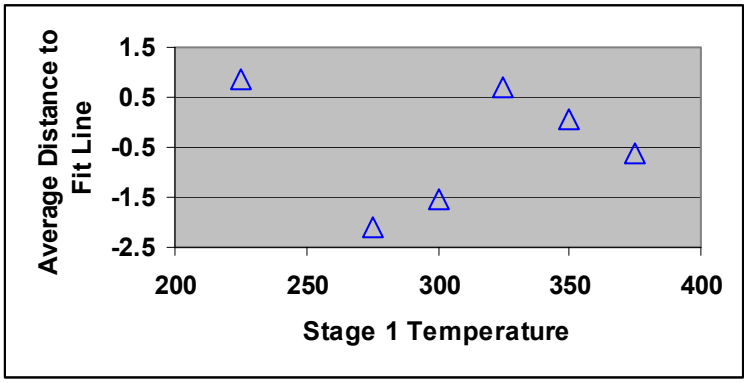

Figure 12: Efficiency variation, corrected for maximum Cu ratio, as a function of stage 1 temperature.

Given the apparent sensitivity of device performance to maximum Cu ratio, several related activities are underway. First, ramifications of this dependency for roll-coater operation are discussed in section 4.a, "Maximum Cu Ratio". Second, in the bell jar, software has been developed to automatically identify the Cu-rich emissivity change via thermopile and to insure that maximum and final Cu-ratios are as consistent and operator-independent as possible. This method of film monitoring was described briefly in the previous annual report, and in a recently-submitted journal article[23] attached to this report. Third, also in the bell jar, a designed experiment examining maximum Cu ratio and atoms deposited in the third stage,[24] is being performed. In this study, a Ga profile very much like that produced in the roll-coaters is utilized, and all deposition variables other than maximum Cu ratio and atoms deposited in stage 3 are maintained at a constant level.

3.c Instantaneous Se-to-Metals Ratio

To examine the effect of variations in instantaneous Se-to-metals ratio experienced in the roll-coaters, CIGS depositions were performed in the bell jar using the roll-coater metals flux profiles described earlier. This progression is illustrated in Figure 13. Figure 13a shows the flux as a function of position (or equivalently time, for the moving production substrate) from a roll-coater Cu source, as described earlier. Figure 13b shows the standard three-stage flux profiles used in the bell jar at ITN. Figure 13c shows the three-stage flux profiles modified to deposit a film of similar composition and thickness, while imitating the flux vs. time seen by a substrate in the roll-coater. The flux profiles of Figure 13c were created by varying with time the setpoint assigned to the electron impact emission spectrometer rate controller.

The insets in Figure 13b and Figure 13c list efficiencies for devices made using each type of flux profile. Work is currently underway to separate and quantify the impacts of deposition rate, instantaneous Se-to-metals ratio, and variability on the results. Furthermore, the flux profiles of Figure 13 should be combined with roll-coater substrate temperature profiles to best simulate then optimize absorber formation in the roll-coaters.

3.d Reproducibility and Comparison to NREL Efficiencies

In Figure 6, Figure 11, and similar data from the bell jar, at least two features of the data warrant further investigation. First, some variability in device performance is evident beyond what can be attributed to variations in maximum Cu ratio or temperature. Although similar (2-3% absolute) variability is a common attribute of published CIGS data, reducing the variability below 0.5% in efficiency is desirable, both to gain understanding of important factors to be controlled during production, and to lessen the number of experiments that must be performed to quantify the impact of a given process variation. Second, the 12% maximum efficiencies in these figures are of course well below the 16+% devices routinely produced in bell jars at NREL. Moving the average efficiency closer to 16% is desirable, both to perform experiments that are consistent with increasing efficiency product goals, and to document the critical process variables that differentiate 12% and 16% efficient co-evaporated devices.

Thus, several examinations were performed to better define sources of variability and of overall efficiency differences when comparing against NREL devices. These examinations included comparisons of:

- Window layer and grid properties among different bell jar (ITN) samples and between ITN and NREL films.
- Physical CIGS characteristics (AES, XRD, SEM, and deposition conditions) among different ITN samples and between ITN and NREL CIGS.
- NREL and ITN substrate effects.

It was found that

- ITN ZnO and ITO properties are reproducible.
- Depositing ITN or NREL window layers on NREL CIGS produces comparable devices.
- Comparisons of physical characteristics (AES, XRD, SEM, or deposition conditions) of 12% and 9% ITN devices and 19% NREL devices do not identify causes for efficiency differences.
- ITN substrates seem to provide less ideal growth conditions for the CIGS film than the NREL substrate. A switch to other substrates is under consideration.
- The ability of the ITN window layers to produce comparable results to the NREL window layers is sensitive to some property of the CIGS.
- Several factors link the poor ITN window layer performance on some CIGS to CdS. Changes to the CBD CdS process to remedy the situation are underway.

The experiments and data leading to these conclusions are described below.

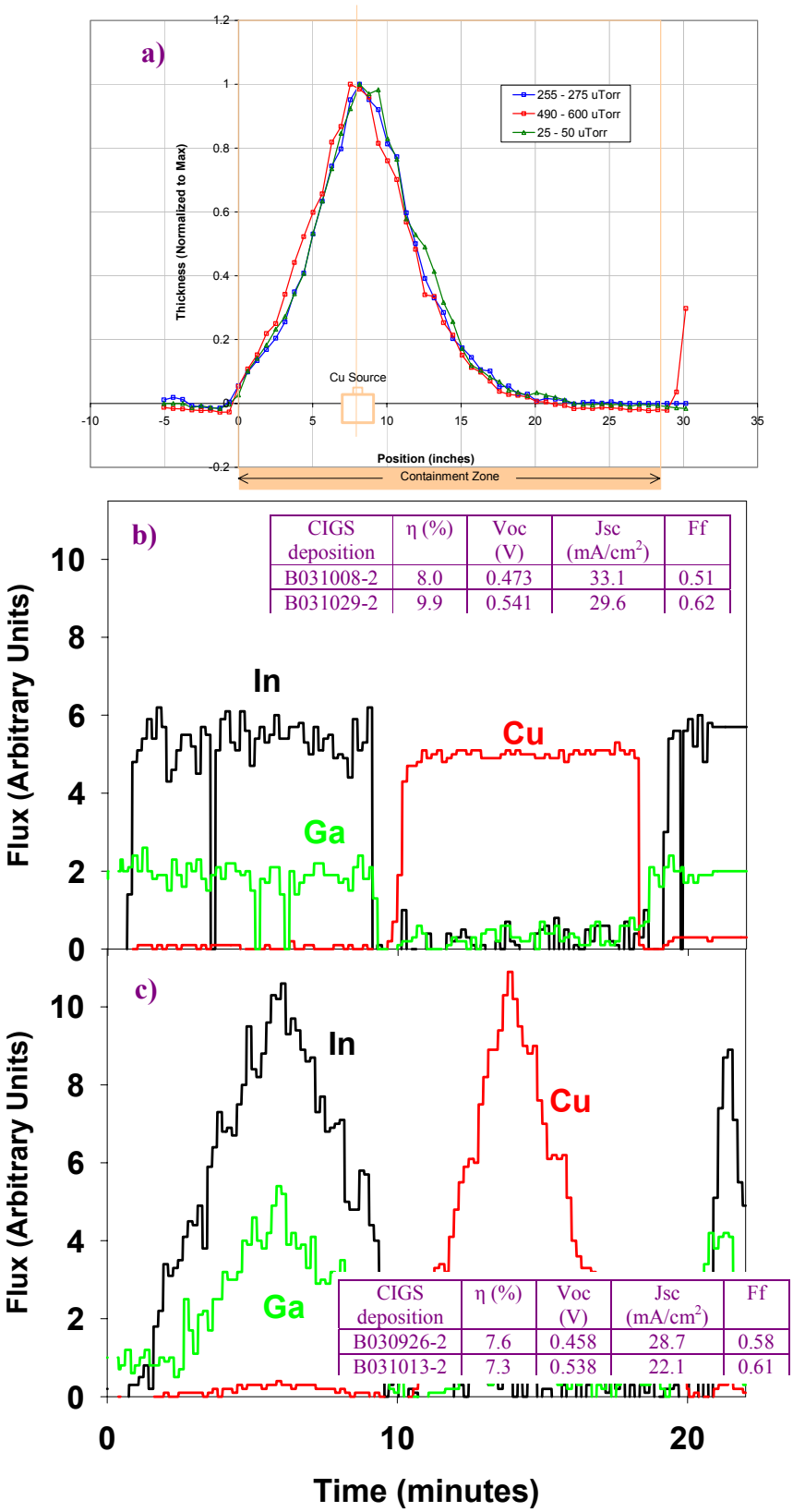

Figure 13: Flux profile a) measured in roll-coater, b) used in bell jar for standard three stage recipe, and c) used in bell jar to imitate roll-coater.

Device finishing was eliminated first as a source for variability and efficiency loss. Witness slides were obtained from TCO depositions yielding 9.5% and 12.5% devices from CIGS films that were expected to be the same. Transmission of the ITO and i-ZnO layers were measured and compared against each other and published data on NREL devices.[15] Grid coverage was also measured. In each case, current losses were quantified by integrating film absorption or grid coverage over the AM1.5 spectrum. Grid geometry and TCO conductivity were used to estimate resistive power loss[25] and resulting efficiency loss. The analysis was performed for an ITN device with 11.8% efficiency (ITN030911), an ITN device with 9.8% efficiency (ITN031108), and published data from NREL on window layers with three different n-ZnO thicknesses: 3600 Å, 4500 Å, 6200 Å. A summary of the analysis is shown in Table 2. Blue areas in the table show window layer losses due to each loss component in absolute percentage points, when applied to 16% efficient CIGS. Yellow areas show resulting device efficiency. It is concluded that window layers should account for less than 1% of the variability between the ITN devices considered, and can account for a loss of only 0.2% to 1.5% when compared to those applied at NREL.

		Sample					
		Perfect windows	**ITN30911**	**ITN31108**	**NREL 3600A**	**NREL 4500A**	**NREL 6200 A**
COMPONENT	**i-ZnO absorption**	0	0	0	0	0	0
	Conductive TCO absorption	0	0.7	1.4	0.3	0.5	0.9
	Grid shading	0	1.0	1.0	0.6	0.6	0.6
	TCO + grid resistance	0	0.1	0.1	0.1	0.0	0.0
	Combined	0	1.8	2.5	1.0	1.1	1.6
	Resulting efficiency:	16%	14.2%	13.5%	15.0%	14.9%	14.4%

Table 2: Summary of window layer loss analysis. Blue areas show window layer losses in absolute percentage points when applied to16% CIGS. Yellow areas show resulting device efficiency.

Experimental verification of the calculations of Table 2 was performed with the help of the NREL CIGS group. A 3" × 3" sample of CIGS grown at NREL was cut into six 1.5" × 1" pieces, with alternate pieces finished into devices simultaneously at NREL or ITN. Table 3 outlines the device results as measured at ITN. Devices finished at either location were comparable: an average of 15.0% for those finished at NREL, versus 14.5% for those finished at ITN.

Sample ID	Efficiency	Voc	Jsc	Fill Factor	Area
1-1	13.58	0.63	31.26	0.69	1.10
1-2	**14.36**	**0.628**	**33.26**	**0.69**	**1.10**
2-1	**14.53**	**0.632**	**31.44**	**0.73**	**0.43**
2-2	12.12	0.624	30.62	0.63	0.43
2-3	11.55	0.614	31.02	0.61	0.43
2-4	14.45	0.621	31.44	0.74	0.43
2-5	6.12	0.517	31.9	0.37	0.43
3-1	**14.57**	**0.642**	**32.48**	**0.7**	**1.10**
3-2	14	0.636	31.9	0.69	1.10
4-1	14.38	0.619	31.47	0.74	0.43
4-2	14.4	0.622	31.16	0.74	0.43
4-3	14.6	0.623	31.67	0.74	0.43
4-4	14.3	0.621	30.94	0.74	0.43
4-5	14.68	0.618	31.61	0.75	0.43
4-6	**14.93**	**0.613**	**33.11**	**0.74**	**0.43**
5-1	**14.43**	**0.632**	**32.48**	**0.7**	**1.10**
5-2	12.81	0.618	32.68	0.63	1.10
6-1	15.33	0.626	32.36	0.76	0.43
6-2	12.18	0.618	30.45	0.65	0.43
6-3	14.98	0.632	31.44	0.75	0.43
6-4	**15.6**	**0.635**	**32.43**	**0.76**	**0.43**
6-5	15.38	0.633	32.12	0.76	0.43
6-6	15.02	0.624	33.08	0.73	0.43

Table 3 : Experimental results of NREL CIGS finished at ITN and NREL. The green higlighted samples were finished at ITN, while the orange highlighted samples were finished at NREL. The best devices on piece sample are in bold.

With window layers ruled out as a cause of variability and efficiency limitation, several characteristics of the CIGS were closely examined. These characteristics included sensor data logged during deposition, AES profiles (measured at University of Illinois), x-ray diffraction (measured at NREL), and SEM. Several aspects of these physical characterization data were self-consistent. For example, SEM showed larger grain size in films that had more Cu-rich growth time. These same films exhibited XRD peaks with narrower full widths at half maximum (FWHM). Also, samples with the same Ga splits between the first and third stages exhibited nearly identical AES Ga profiles. However, none of the data yielded correlations with efficiency. Even when NREL flux and temperature profiles were exactly reproduced in the bell jar at ITN, resulting device efficiencies still fell into the typical 11-12% range. As physical characterization of the CIGS was not helpful in identifying causes for efficiency differences, those data are not presented in detail in this report.

Thus, subsequent experiments focused on the substrate and back contact. With the help of the NREL CIGS group, some trials with different substrates and window layers were performed. These experiments and results are summarized in Table 3. The combination of NREL glass and Mo, NREL CIGS, and NREL window layers yielded a substrate with device efficiencies averaging 17.2% (blue portion of table). When ITN Mo and glass is substituted for the substrate in this structure, average efficiency is reduced to 13.0% (yellow portion of table). Surprisingly, when ITN window layers are applied to the same CIGS, efficiency is further reduced to 9.2%. This magnitude of window layer efficiency loss contradicts the earlier comparison performed in Table 3. Thus, two conclusions can be drawn from the data of Table 3. First, the ITN substrate seems to provide less ideal growth conditions for the CIGS film than the NREL substrate. Second, the ability of the ITN window layers produce comparable results to the NREL window layers is sensitive to some property of the CIGS.

Cell #	n	Voc	Jsc	ff
NREL glass & Mo + NREL CIGS deposition S2212 + NREL device finishing				
1	16.4	0.683	30.9	77.4
2	17.4	0.683	32.8	77.7
3	16.1	0.677	33.0	72.2
4	17.4	0.678	33.1	77.6
5	17.2	0.674	33.2	76.8
6	17.5	0.693	32.5	77.8
7	17.7	0.694	32.8	77.8
8	17.6	0.693	32.8	77.4
9	17.5	0.691	32.8	77.4
10	17.6	0.690	32.9	77.7
Averages:	17.2	0.686	32.7	77.0
ITN glass & Mo + NREL CIGS deposition S2215 + NREL device finishing				
1	12.7	0.619	31.5	65.2
2	13.2	0.618	32.7	65.6
3	13.2	0.616	32.5	65.8
4	12.7	0.614	31.9	64.7
5	12.7	0.614	31.5	65.5
6	12.2	0.616	31.6	62.6
7	13.0	0.628	31.2	66.4
8	13.2	0.628	31.4	66.7
9	13.4	0.627	31.8	67.2
10	13.2	0.626	31.2	67.5
11	13.4	0.624	31.9	67.2
Averages:	13.0	0.621	31.7	65.9
ITN glass & Mo + NREL CIGS deposition S2215 + ITN device finishing				
1	8.2	0.604	28.7	47.0
2	10.5	0.601	31.6	55.0
3	10.0	0.592	30.1	56.0
4	8.5	0.599	26.8	53.0
5	9.8	0.596	29.1	57.0
6	7.7	0.599	30.0	45.0
7	9.5	0.599	30.8	52.0
Averages:	9.2	0.599	29.6	52.1

Table 4: Comparison of device efficiencies with different substrates and window layers

Several characteristics of the data implicate the CdS in the ITN / NREL window layer efficiency difference. First, because ITN's i-ZnO and ITO are sputtered from 18" targets, it is unlikely that they could provide the cm-scale nonuniformity in materials properties necessary to create the device-to-device variations seen in the green portion of Table 4. Second, significant differences in voltage and shunt resistance exist between the ITN-finished and NREL finished devices on the same CIGS. It is difficult to imagine how the TCO's would have a strong effect on voltage and shunt resistance, rather than J_{sc} and series resistance alone. Third, quantum efficiency of ITN-finished devices has significantly less absorption at 450 nm than published NREL data,[26] despite use of the same recipe and procedure. Several changes to the CdS procedure at ITN are currently being evaluated.

Best choice of substrate is also under evaluation, based on the comparison between the yellow and blue portions of Table 4. Glass has been utilized in most of the bell jar experiments under this program, since it can support a thermocouple, provides Na to the growing film, is smooth, and does not out-diffuse Fe or other metals. However, if the current substrates are limiting device efficiencies or contributing to variability, other choices may be more attractive. Steel and Al_2O_3 are under consideration as alternate "baseline" substrates. Once the CdS procedure is determined to be optimized, CIGS will also be deposited on glass + Mo from NREL, for comparison. Illuminating the role of the substrate in absorber formation not only provides a path for experiments at increased efficiencies with decreased variability, but also provides a foundation for optimization substrate-related properties that are important to production, such as amount of Na precursor or back contact characteristics.

4 Application To Production Roll-Coaters

The final major task in this program is applying process sensivity information gained in the bell jar to the production environment. In the sections below, work in the roll-coaters related to maximum Cu ratio and post CIGS handling are discussed.

4.a Maximum Cu Ratio

Given the sensitivity of bell jar devices to maximum Cu ratio (section 3.b), tests of the impact of maximum Cu ratio are also underway in the production systems. A two-level screening test of Cu-rich excursion and final Cu/(Ga+In) was performed in one of the CIGS production chambers (CIGS3) on lot 1472SA. The 2 × 2 matrix was replicated one time for a total of eight test conditions. The planned levels for Cu-rich excursion were 1.0 and 1.1, as measured by in-situ XRF. The planned levels for final composition (Cu/(Ga+In)) were 0.81 and 0.91. The web was processed according to baseline process conditions through production cell (i.e., large area devices, total area 78 cm^2) fabrication and measurement. Three sample panels were extracted from each condition, for a total of thirty sample cells for each. Deletion of outliers well outside the normal distribution was performed prior to analysis.

The mean IV characteristics of each condition are plotted on the interaction charts in Figure 14. For films processed without a Cu-rich excursion (in process Cu/(Ga+In) ~ 1.0), the final composition had a significant effect on final efficiency; a final Cu/(Ga+In) of 0.91 was superior to 0.81. All IV parameters (V_{oc}, I_{sc}, and fill factor) improved. For films that experienced a Cu-rich excursion (in process Cu/(Ga+In) ~ 1.1), the efficiency was much less dependent on the final Cu/(Ga+In). The latter process was more robust, although the mean efficiency under the best conditions may be slightly lower than the case where the film did not go Cu-rich.

Efforts to apply thermopile sensing of the Cu-rich growth excursion in the production systems, similar to what has been implemented in the bell jar, are also underway.

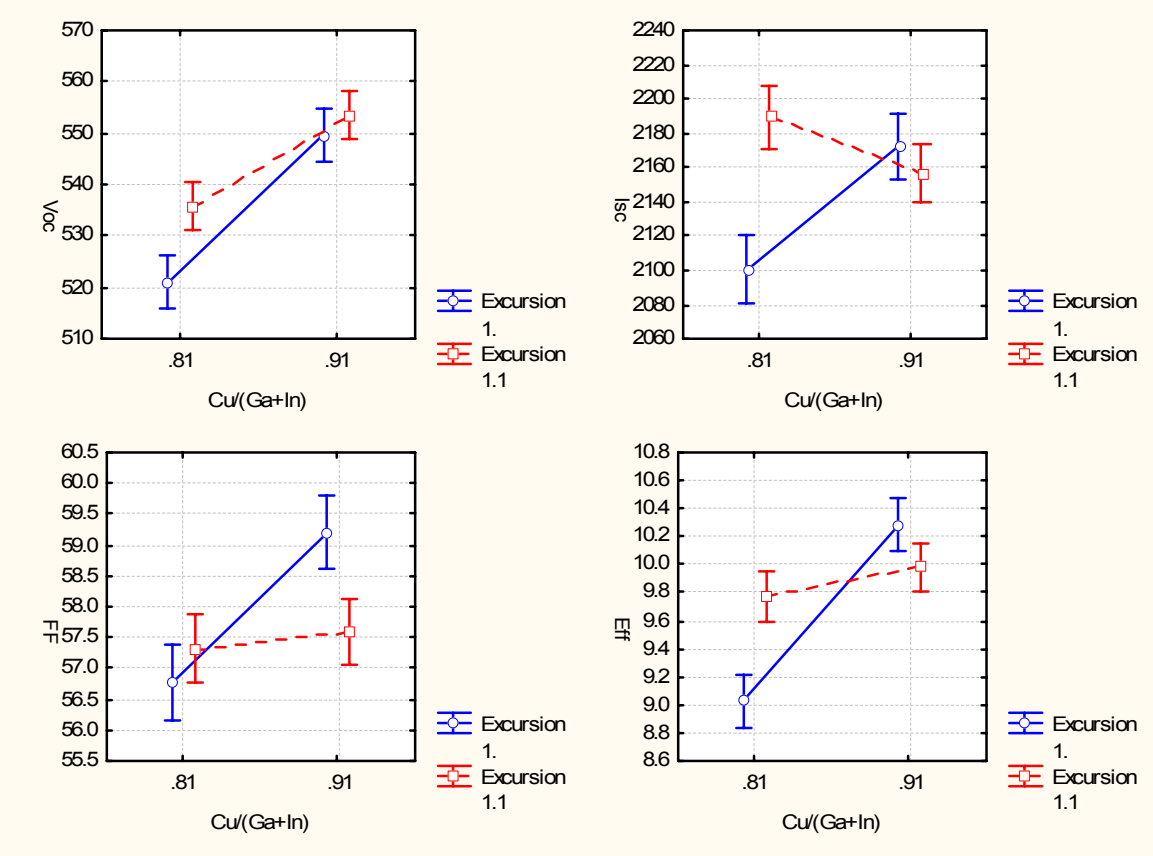

Figure 14: Interaction charts summarizing device parameters from roll-coaters as a function of maximum and final Cu ratio.

As a preliminary test in a production system, a thermopile was installed in a post-deposition zone. Results from these initial tests were mixed. As expected, the IR sensor did show an increase in signal for Cu ratios exceeding one. Figure 15 shows an example of composition and IR sensor data from the roll-coater. The system was perturbed at 6500 seconds to verify that when Cu ratio exceeds one (in green, as measured by XRF), the signal from the IR sensor (in red) increases. However, the signal increase is a smaller fraction of the total signal than when the sensor is used in the bell jar, most likely due to the elevated operating temperature in the roll-coater. Furthermore, after approximately 50 hours of deposition, the IR sensor failed due to disintegration of the optics.

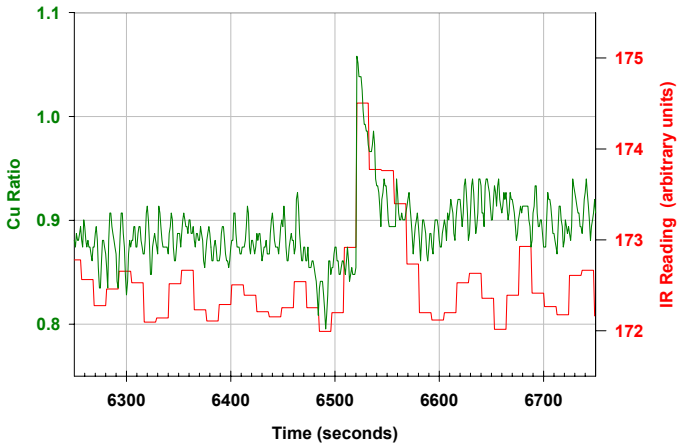

Figure 15: Example of data from initial IR sensor tests in production roll-coater.

The thermopile optics were modified to withstand higher temperatures and installed in the CIGS4 production roll-coater, between stages 2 and 3. An example of thermopile signal as a function of web position is shown in Figure 16. The thermopile was found to be irresponsive after approximately 200 hours of deposition. Some sensor cooling may be necessary to control temperature in this harsh environment, both to increase sensor lifetime and to more easily separate out signal background due to elevated sensor temperature. Current efforts are focused on weighing the expected impact on device performance against the necessity to control temperature and apply more complex analysis.

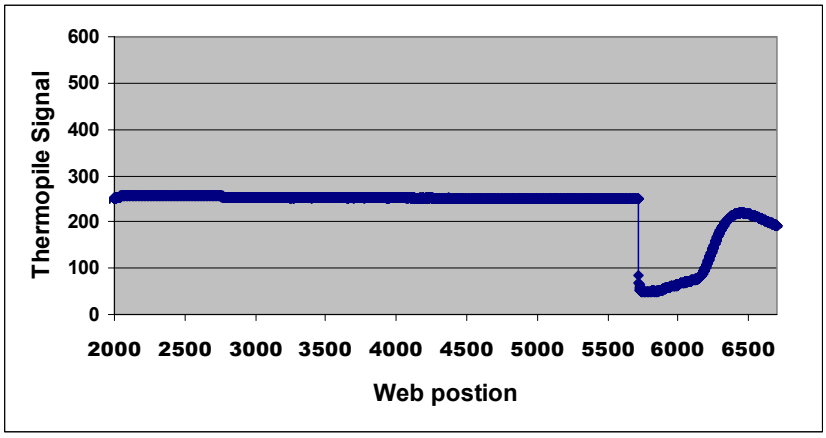

Figure 16: Thermopile signal versus web position for production deposition G40396.

4.b Post-CIGS Deposition Conditions

Several procedures relevant to handling of devices after CIGS deposition were examined. These conditions included exposure time to air prior to CdS deposition, stability of TCO layers, and effect of thioacetamide treatment prior to CdS.

Sensitivity of device performance to air exposure time between CIGS and CdS processing was examined. Long exposure times were examined using the production systems at GSE, while very short exposure times were examined using the bell jar at ITN (section 3.a). Data from the production systems are shown in Figure 17, where each position corresponds to 200 individual small area (0.68 cm^2) devices randomized over 20 sq. ft. of substrate/absorber. Post CdS window layer completion was performed simultaneously for all devices under standard production conditions. Squares indicate the mean value of each device parameter as a function of air exposure time. Error bars indicate ±95% confidence intervals based on the distribution of devices made under one condition. Slight downward trends in efficiency and fill factor with increasing air exposure time are evident. It should be noted that although plotted on a linear scale, the air exposure time scale (x-axis) is not linear. According to these results, longest times explored should therefore be avoided when scheduling processing steps.

In a joint study with the National Renewable Energy Laboratory (NREL) and the Institute for Energy conversion (IEC), the effects of damp heat exposure on window layer characteristics were examined. Unprotected bi-layers from IEC, NREL, and GSE were exposed to damp heat at 85 °C and 85% relative humidity for varying lengths of time at GSE. Sheet resistance and transmission were measured periodically. Samples from IEC were i-ZnO/ITO on soda-lime or 7059 glass. Samples from NREL were i-ZnO/ZnO:Al on soda-lime or 7059 glass. The GSE specimens represent i-ZnO/ITO on soda-lime glass (SLG). Results are shown in Figure 18. As seen in Figure 18a, no changes in transmission above measurement uncertainty are observed. However, several samples exhibited significant changes in sheet resistance, as seen in Figure 18b. Most notably, the NREL bi-layer exhibited about a factor of two increase in sheet resistance on SLG, and about a 30% increase in sheet resistance on 7059. The IEC bi-layer on SLG showed a 20% increase in sheet resistance, whereas the IEC bi-layer on 7059 glass showed no measurable change in resistance. The GSE layers also displayed no measurable change.

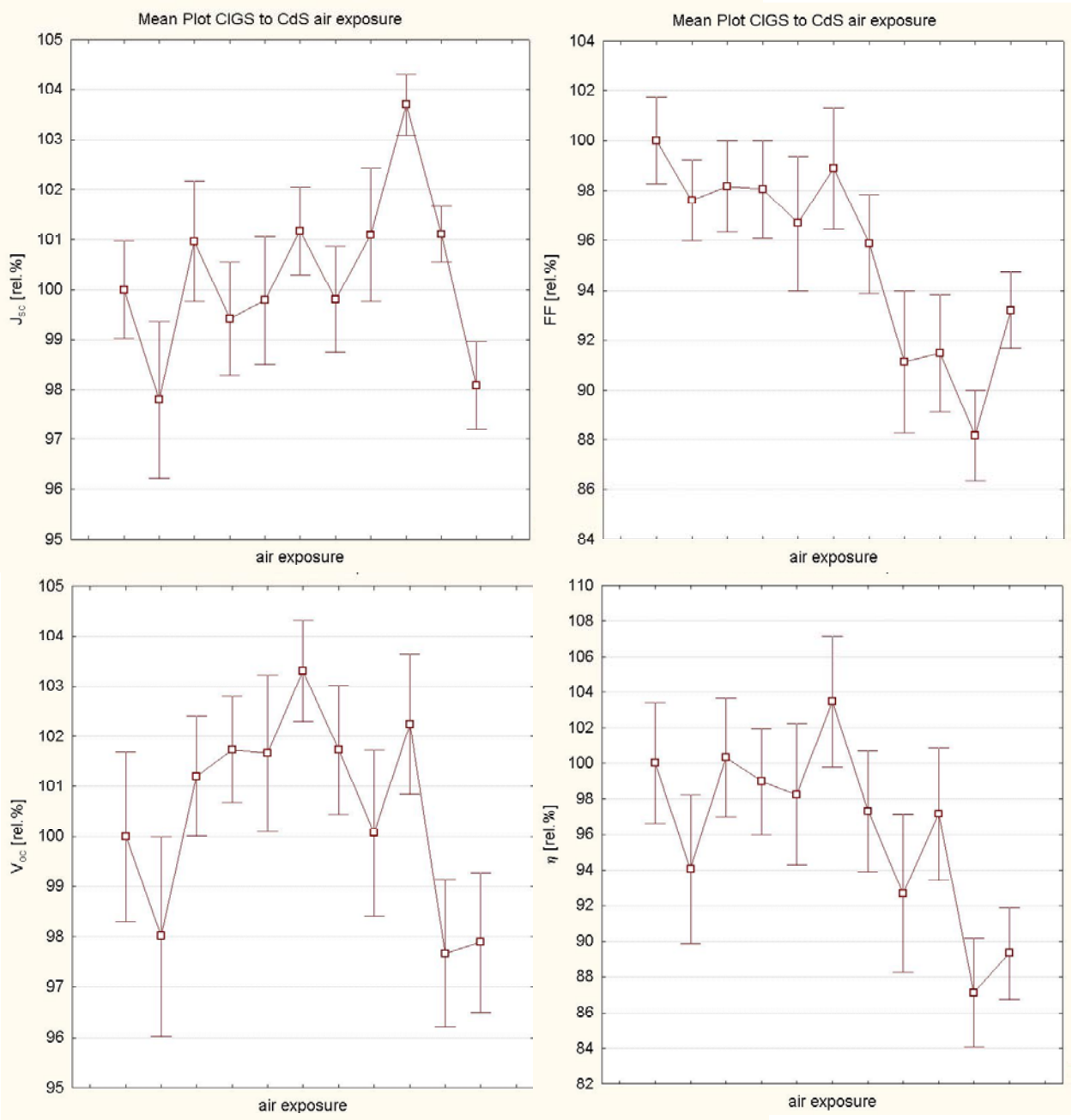

Figure 17: Device parameters as a function of air exposure time between CIGS and CdS processing.

Error bars in Figure 18 represent 95% confidence intervals for the mean of the sample set. The error bars appear large for some sample sets because the means of those sets are not well-defined, due to small numbers of samples with varying sheet resistances. The large error bars are *not* indicative of larger measurement error or erratic fluctuations in the properties of one sample with time. Thus, for the samples measured, resistance stability depends most strongly on the bi-layer deposition process as well as the TCO material. For samples that degrade, those on SLG degrade more than those on 7059 glass, suggesting that Na may play a role. To this end, the data strengthens the confidence into the GSE window layer with respect to product longevity.

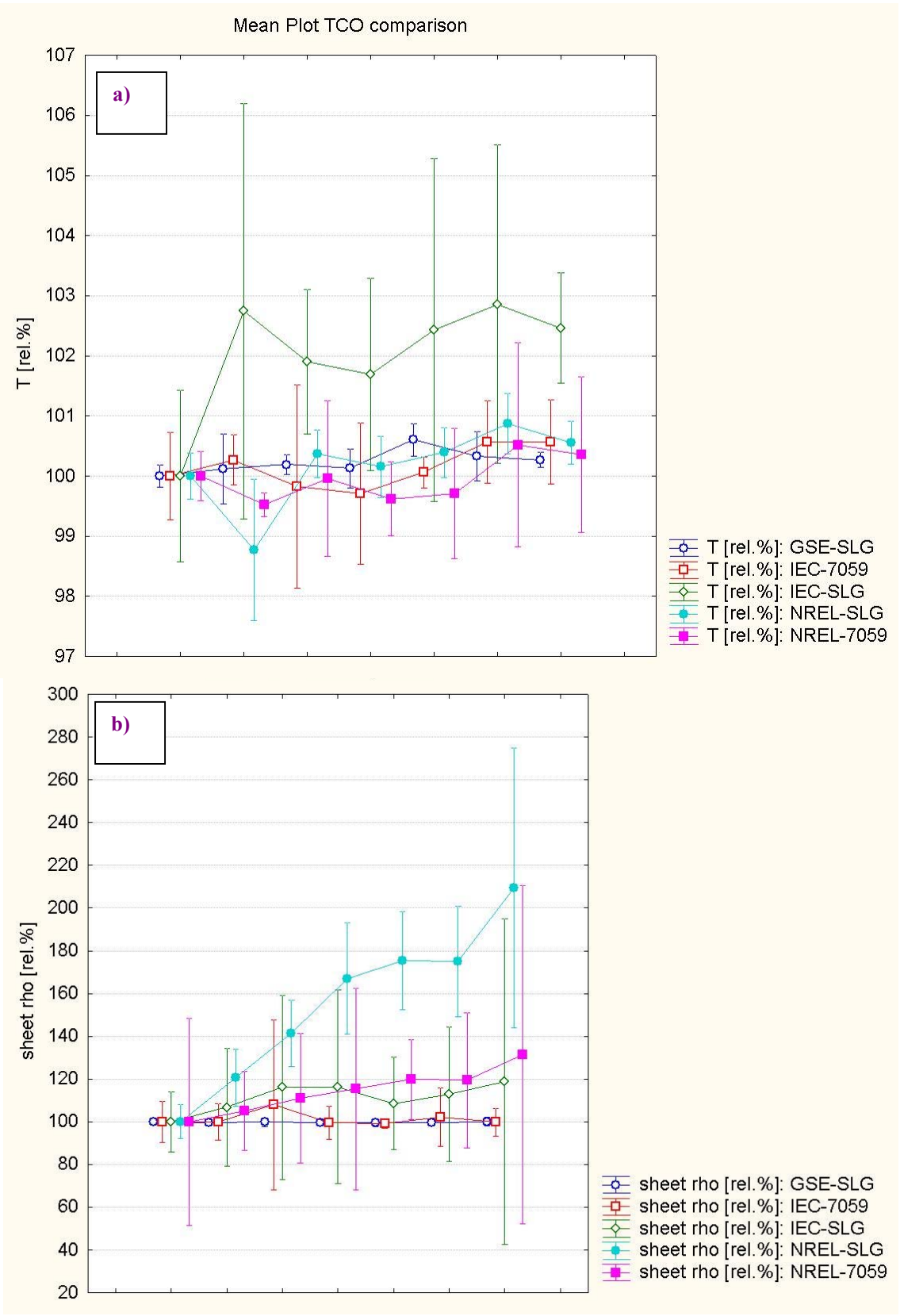

Figure 18: a) Transmission and b) sheet resistance as a function of time for different bi-layers.

CIGS surface passivation and improved junction formation is being investigated via thioacetamide treatment.[27,28] Design of experiments is being used to optimize treatment temperature, time, concentrations, and salt for the GSE production material. Results will be reported when analysis of the experimental matrices is complete.

5 Technical Summary

Work during Phase II progressed in three major areas: production system characterization, quantification of process sensitivities in the bell jar, and application of results to the production roll-coaters.

The following conclusions were drawn related to production system characterization:

- Metals flux profiles agree well with the expected $\cos^3\theta$ distribution and are unaffected by Se pressures.
- Se impingement rates were derived from sensor data.
- Thermocouple data was used to estimated temperature profiles.

The following conclusions were drawn related to quantification of process sensitivities in the bell jar:

- Over the range examined there is no measureable impact of cool-down rate, cool-down Se flux, or venting temperature on device performance.
- No efficiency gain is realized by shortening the time between venting and CdS
- For devices with low final Cu ratio ($R_3 \leq 0.9$), device efficiency improves continuously with maximum Cu ratio approaching 1.15.
- By the time maximum Cu ratio reaches 1.3, a significant decrease in efficiency is observed.
- Efficiency falls off as final Cu ratio approaches 1, but some samples tolerate a higher final Cu ratio than others. The controlling condition for limit on maximum final Cu ratio is not apparent from the present data.
- Bell jar metals flux profiles can be modified to imitate roll-coater flux profiles.
- The ZnO and ITO used in bell jar devices are reproducible, and depositing them or NREL window layers on NREL CIGS produces comparable devices.
- However, the ability of the bell jar (ITN) window layers produce comparable results to the NREL window layers is sensitive to some property of the CIGS. Several factors implicate the CdS in this sensitivity.
- Bell jar (ITN) substrates seem to provide less ideal growth conditions for the CIGS film than the NREL substrate. A switch to other substrates is under consideration.

The following conclusions were drawn related to applying process sensitivity information to the production environment:

- A two-level screening test in the production systems indicate that a process containing reaching a maximum Cu ratio of 1.1 is more robust than one in which maximum Cu ratio is 1.0.
- However, for a maximum Cu ratio reach 1.1, the mean efficiency under the best conditions may be slightly lower than the case where the film did not go Cu-rich.
- A thermopile has been installed in a roll-coater to sense the extent of the Cu-rich growth excursion.
- The expected impact on device performance must be weighed against the necessity to control temperature and apply more complex analysis for this sensor.
- Sensitivity of device performance to air exposure time between CIGS and CdS processing was examined. The longest times explored should be avoided when scheduling processing steps.
- GSE TCO's are stable with exposure to damp heat.

- CIGS surface passivation and improved junction formation are being investigated via thioacetamide treatment of production material.

6 Future Directions

During Phase II, work focused on completing characterization of the metals and Se fluxes in the production roll-coaters, examining three-stage process sensitivities in the bell jar, and beginning to apply this information to the roll-coaters.

Phase III tasks will build on this year's results. In the bell jar, several process sensitivity investigations will be concluded, and some new ones begun. These investigations will include use of less expensive source materials, decreased deposition times, variations in instantaneous Se to metals ratio as implied by the roll-coater flux profiles, optimization of Na precursor at roll-coater conditions, and resolution of CdS issues. Where applicable these new results will be applied in the production roll-coaters to demonstrate process improvement. Appropriate actions based on this year's maximum Cu ratio and thioacetamide treatment data will also be defined and implemented.

7 Team Activities

GSE takes part in CIS National Team activities. Recent contributions have included participation in and presentations at team meetings, submission of samples for comparative absorber studies, and review and discussion of related data.

8 Phase II Publications, Presentations, and Reports

The following publications, presentations, and reports were generated related to this contract during Phase II. They are listed in chronological order:

1. Phase II, First Quarterly Report, September 1, (2003).
2. J. Britt, "Tolerance of Three-Stage Deposition to Variations Imposed by Roll-toRoll Manufacture", Presentation at August 2003 Photovoltaics Subprogram Peer Review.
3. Phase II, Second Quarterly Report, November, 24, (2003).
4. Phase II, Third Quarterly Report, February 26, (2004).
5. I.L. Repins, D. Fisher, W.K. Batchelor, L. Woods, M.E. Beck, "A Non-Contact Low-Cost Sensor for Improved Repeatability in Co-Evaporated CIGS", submitted to *Progress in Photovoltaics*, May 2004.

9 References

[1] J.R. Tuttle, M.A. Contreras, K.R. Ramanathan, S.E. Asher, R. Bhattacharya, T.A. Berens, J. Keane, R. Noufi, "Materials and Processing Issues in Thin-Film Cu(In,Ga)Se_2!Based Solar Cells", *AIP Conference Proceedings 394*, 83-105 (1996).

[2] Hedstrom, H. Ohlsen, M. Bodegard, A. Kylner, L. Stolt, D. Hariskos, M. Ruckh, H.W. Schock, *Proceedings of the 23rd IEEE Photovoltaics Specialists Conference*, 364-371 (1993).

[3] W.N. Shafarman, R.W. Birkmire, M. Marudachalam, B.E. McCandless, J.M. Schultz, "Fabrication and Characterization of Cu(In,Ga)Se2 Solar Cells with Absorber Bandgap from 1.0 to 1.5 eV", *AIP Conference Proceedings 394*, 123-131 (1996).

[4] T. Wada, S. Hayashi, Y. Hashimoto, S. Nishiwaki, T. Sato, T. Negami, M. Nishitani, "High Efficiency Cu(In,Ga)Se_2 (CIGS) Solar Cells with Improved CIGS Surface", *Proceedings of the 2nd World Conference and Exhibition on Photovoltaic Energy Conversion*, pp. 403-408, 1998.

[5] B. Dimmler, E. Gross, D. Hariskos, F. Kessler, E. Lotter, M. Powalla, J. Springer, U. Stein G. Voorwinden, M. Gaeng, S. Schleicher, "CIGS Thin Film Module Technology: Towards Commercialization", *Proceedings of the 2nd World Conference and Exhibition on Photovoltaic Energy Conversion*, pp. 419-423, 1998.

[6] W.N. Shafarman, R.W. Birkmire, S. Marsillac, M. Marudachalam, N. Orbey, T.W.F Russell, "Effect of Reduced Deposition Temperature, Time, and Thickness, on Cu(In,Ga)Se_2 Films and Devices", *Conference Record of the 26th IEEE Photovoltaic Specialists Conference*, pp.331-334, (1997).

[7] W.N. Shafarman, J. Zhu, "Effect of Substrate Temperature and Deposition Profile on Evaporated Cu(In,Ga)Se_2 films and devices", *Thin Solid Films* **361-362**, pp. 473-477, (2000).

[8] S. Nishiwaki, T. Satoh, S. Hayashi, Y. Hashimoto, T. Negami, T. Wada, "Preparation of Cu(In,Ga)Se_2 thin films from In-Ga-Se Precursors for high-efficiency solar cells", *Journal of Materials Research* **14** (12), pp. 4514-4520, (1999).

[9] J.R. Tuttle, T.A. Berens, J. Keane, K.R. Ramanathan, J. Granata, R.N. Bhattacharya, H. Wiesner, M.A. Contreras, R. Noufi, "Investigations into Alternate Substrate, Absorber, and Buffer Layer Processing for Cu(In,Ge)Se_2 – Based Solar Cells", *Conference Record of the 25th IEEE Photovoltaic Specialists Conference*, pp.797-800, (1996).

[10] J.E. Granata, "The Impact of Deliberate Sodium Incorporation on $CuInSe_2$-Based Solar Cells", Unpublished Ph.D. Thesis, Colorado State University, (1999).

[11] M. Bodegard, J. Kessler, O. Lundberg, J. Scholdstrom, L Stolt, "Growth of Co-Evaporated Cu(In,Ga)Se_2 – The Influence of Rate Profiles on Film Morphology," *Materials Research Society Symposium Proceedings*, **668**, (2001), pp. H2.2.1-H2.2.12.

[12] A.M. Gabor, J.R. Tuttle, D.S. Albin, M.A. Contreras, R. Noufi, A.M. Herman, "High-efficiency $CuIn_xGa_{1-x}Se_2$ solar cells made from $(In_x,Ga_{1-x})_2Se_3$ precursor films", *Applied Physics Letters*, **65**(2), pp. 198-200, (1994).

[13] "Tolerance of Three-Stage CIGS Deposition to Variations Imposed by Roll-to-Roll Manufacturing," *Phase I Annual Report to NREL under Subcontract ZDJ-2-30630-14*, (2003).

[14] R.W. Birkmire, W.N. Shafarman, E. Eser, S.S. Hegedus, B.E. McCandless, R. Aparicio, K. Dobson, "Optimization of Processing and Modeling Issues for Thin Film Solar Cell Devices Including Concepts for the Development of Polycrystalline Multijunctions", *Annual Report to NREL under Subcontract ZAK-8-17619-33*, 2001, pp. 3-4.

[15] M.A. Contreras, J. Tuttle, A. Gabor, A. Tennant, K. Ramanathan, S. Asher, A. Franz, J. Keane, L. Wang, J. Scofield, R. Noufi, "High Efficiency Cu(In,Ga)Se_2-Based Solar Cells: Processing of Novel Absorber Structures," *First World Conference on Photovoltaic Energy Conversion*, (1994), pp. 68-75.

[16] Noufi, et al.

[17] T. Walter et al, *Proceedings of the 13th European PVSEC*, (1995), pg. 1999.

[18] I.L. Eisgruber, J.E. Granata, J.R. Sites, J.Hou, J. Kessler, "Blue Photon Modification of Diode Barrier in $CuInSe_2$ Solar Cells", *Solar Energy Materials and Solar Cells*, **53**, pp. 367-377, 1998.

[19] L. Kronik. U. Rau, D. Cahen, "Interface redox engineering of Cu(In,Ga)Se2 based solar cells: oxygen, sodium, and chemical bath effects", *Thin Solid Films*, vol. **361/362**, (2000), pp. 353.

[20] D. S. Albin, G.D. Mooney, A. Duda, J. Tuttle, R. Matson, R. Noufi, *Solar Cells* **30**, 47, (1991).

[21] B. M. Keyes, P. Dippo, W. Metzger, J. AbuShama, R. Noufi, "Cu(In,Ga)Se_2 Thin Film Evolution During Growth – A Photoluminescence Study", *Conference Record of the Twenty-Ninth IEEE Photovoltaics Specialists Conference*, (2002).

[22] J.R. Tuttle, J.R. Sites, A. Delahoy, W. Shafarman, B. Basol, F. Fonash, J. Gray, R. Menner, J. Phillips, A. Rockett, J. Scofield, F.R. Shapiro, P. Singh, V. Suntharalingam, D. Tarrant, T. Walter, S. Wiedeman, T.M. Peterson, "Characterization and Modeling of Cu(In,Ga)$(S,Se)_2$-based Photovoltaic Devices: A Laboratory and Industrial Perspective," *Progress in Photovoltaics: Research and Applications*, **3**, pp. 89-104, (1995).

[23] I.L. Repins, D. Fisher, W.K. Batchelor, L. Woods, M.E. Beck, "A Non-Contact Low-Cost Sensor for Improved Repeatability in Co-Evaporated CIGS", submitted to *Progress in Photovoltaics*, May 2004.

[24] A.M. Gabor, "The Conversion of $(In,Ga)_2Se_3$ Thin Films to Cu(In,Ga)Se_2 for Application to Photovoltaic Solar Cells", PhD Thesis, University of Colorado, (1995). See pg. 122, figure 6.3.

[25] Martin Green, *Solar Cells*, Prentice-Hall, 1982, pp.145 ff.

[26] M. A. Contreras, B. Egaas, K. Ramanathan, J. Hiltner, A. Swartzlander, F. Hasoon, R. Noufi, "Progress toward 20% efficiency in Cu(In,Ga)Se2 polycrystalline thin-film solar cells," *Progress in Photovoltaics: Research and Applications*, **7** (4), (1999), pp 311-316.

[27] T. Wada, Y. Hashimoto, S. Nishiwaki, T. Satoh, S. Hayashi, T. Negami, H. Miyake, "High efficiency CIGS solar cells with modified CIGS surface," *Sol. En. Mtls. & Sol. Cells*, **67**, (2001), pp. 305-310.

[28] T. Nakada, K. Matsumoto, M. Okumura, "Improved Efficiency of Cu(In,Ga)Se_2 Thin Film Solar Cells by Surface Sulfurization Using Wet Process," *Proc. of the 29th IEEE PVSC*, (2002).